Lead-Lag Control for Helicopter Vibration and Noise Reduction
Summary of Research
NASA Langley Research Center (LaRC) Research Grant NAG-1-2050

Dr. Farhan Gandhi
Department of Aerospace Engineering, The Pennsylvania State University

Introduction

As a helicopter transitions from hover to forward flight, the main rotor blades experience an asymmetry in flow field around the azimuth, with the blade section tangential velocities increasing on the advancing side and decreasing on the retreating side (Figure 1). To compensate for the reduced dynamic pressure on the retreating side, the blade pitch angles over this part of the rotor disk are increased. Eventually, a high enough forward speed is attained to produce compressibility effects on the advancing side of the rotor disk and stall on the retreating side. The onset of these two phenomena drastically increases the rotor vibratory loads and power requirements, thereby effectively establishing a limit on the maximum achievable forward speed. The alleviation of compressibility and stall (and the associated decrease in vibratory loads and power) would potentially result in an increased maximum forward speed.

In the past, several methods have been examined and implemented to reduce the vibratory hub loads. Some of these methods are aimed specifically at alleviating vibration at very high flight speeds and increasing the maximum flight speed, while others focus on vibration reduction within the conventional flight envelope. Among the later are several types passive as well as active schemes. Passive schemes include a variety of vibration absorbers such as mechanical springs [1], pendulums [2], and bifilar absorbers [3]. These mechanism are easy to design and maintain, but incur significant weight and drag penalties. Among the popular active control schemes in consideration are Higher Harmonic Control (HHC) and Individual Blade Control (IBC). HHC uses a conventional swash plate to generate a multi-cyclic pitch input to the blade [4-5]. This requires actuators capable of sufficiently high power and bandwidth, increasing the cost and weight of the aircraft [6]. IBC places actuators in the rotating reference frame, requiring the use of slip rings capable of transferring enough power to the actuators. Both schemes cause an increase in pitch link loads [7]. Trailing Edge Flap (TEF) deployment can also used to generate unsteady aerodynamic forces and moments that counter the original vibratory loads, and thereby reduce rotor vibrations.

While the vibrations absorbers, HHC, IBC, and TEF concepts discussed above attempt to reduce the vibratory loads, they do not specifically address the phenomena causing the vibrations at high advance ratios. One passive method that attempts to directly alleviate compressibility and stall, instead of reducing the ensuing vibrations, is the use of advanced tip designs. Taper, sweep, anhedral, and the manipulation of other geometric properties of the blade tips can reduce the severity of stall and compressibility effects [8,9], as well as reduce rotor power [10]. A completely different approach to solve these problems is the tiltrotor configuration. As the forward velocity of the aircraft increases, the rotors, in this case, are tilted forward until they are perpendicular to the flow and act as propellers. This eliminates the edgewise flow encountered

by conventional rotors [11] and circumvents all the problems associated with flow asymmetry. However, the success involves a tremendous increase in cost and complexity of the aircraft.

Another possible approach that has been proposed for the alleviation of vibratory loads at high forward flight speeds involves the use of controlled lead-lag motions to reduce the asymmetry in flow. A correctly phased 1/rev controlled lag motion could be introduced such that it produces a backward velocity on the advancing side and a forward velocity on the retreating side, to delay compressibility effects and stall to a higher advance ratio. Using a large enough lead-lag amplitude, the tip velocities could be reduced to levels encountered in hover (See Figure 2).

This concept was examined by two groups in the 1950's and early 1960's. In the United States, the Research Labs Division of United Aircraft developed a large lead-lag motion rotor, meant to achieve lag motion amplitudes up to 45°. In order to reduce the required actuation force, the blade hinges were moved to 40% of the blade radius to increase the rotating lag frequency to approximately 1/rev. The blade hinges were redesigned to produce a flap-lag coupling so the large flapwise aerodynamic loads could be exploited to actuate the blades in the lag direction [12, 13]. A wind tunnel test of this rotor concept revealed actuation and blade motion scheduling problems. The project was eventually discontinued due to these problems and high blade stresses.

Around the same time, at Boelkow in Germany, a similar lead-lag rotor program was conducted under the leadership of Hans Derschmidt. Here, too, the blade hinges were moved outboard to 34% radius to reduce the actuation loads [14]. The main difference between this and the United Aircraft program was the use of a mechanical actuation scheme with maximum lead-lag motions of 40°. This program was also discontinued for unclear reasons.

The present study is directed toward conducting a comprehensive analytical examination to evaluate the effectiveness of controlled lead-lag motions in reducing vibratory hub loads and increasing maximum flight speed. Since both previous studies on this subject were purely experimental, only a limited data set and physical understanding of the problem was obtained. With the currently available analytical models and computational resources, the present effort is geared toward developing an in-depth physical understanding of the precise underlying mechanisms by which vibration reduction may be achieved. Additionally, in recognition of the fact that large amplitude lead-lag motions would - (i) be difficult to implement, and (ii) produce very large blade stresses; the present study examines the potential of only moderate-to-small lead-lag motions for reduction of vibratory hub loads. Using such an approach, the emphasis is not on eliminating the periodic variations in tangential velocity at the blade tip, but at best reducing these variations slightly so that compressibility and stall are delayed to slightly higher advance ratios.

This study was conducted in two steps. In the first step, a hingeless helicopter rotor was modeled using rigid blades undergoing flap-lag-torsion rotations about spring restrained hinges and bearings. This model was then modified by separating the lead-lag degree of freedom into two components, a free and a prescribed motion. Using this model, a parametric study of the effect of phase and amplitude of a prescribed lead-lag motion on hub vibration was conducted. The data gathered was analyzed to obtain an understanding of the basic physics of the problem

and show the capability of this method to reduce vibration and expand the flight envelope. In the second half of the study, the similar analysis was conducted using an elastic blade model to confirm the effects predicted by the simpler model.

Analytical Models

Rigid Blade Model

The rotor aeroelastic model used in the present study assumes that the blades undergo rigid flap-lag-torsion rotations about spring-restrained hinges/bearings. The virtual hinge location and spring rates are selected to simulate the fundamental natural frequencies of a typical hingeless rotor. The nondimensional coupled flap-lag-torsion equations of motion of the rotor blade can then be written as:

$$\ddot{\beta}+\nu_\beta^2\beta-I_x^*\ddot{\theta}-I_x^*\theta-2\beta\dot{\zeta}=\frac{M_\beta^{aero}}{I_\beta\Omega^2} \tag{1}$$

$$\ddot{\zeta}+\nu_\zeta^2\zeta+2\beta\dot{\beta}-2I_x^*\beta\dot{\theta}+2\xi\nu_\zeta\dot{\zeta}=\frac{M_\zeta^{aero}}{I_\beta\Omega^2} \tag{2}$$

$$I_f^*\ddot{\theta}-2I_x^*\ddot{\beta}+I_f^*\nu_\theta^2\theta-I_x^*\beta+2I_x^*\beta\dot{\zeta}=\frac{M_\theta^{aero}}{I_\beta\Omega^2} \tag{3}$$

Evaluation of the aerodynamic flap, lag, and torsion moments on the right hand side of the above equations requires the calculation of the sectional lift, drag, and pitching moment coefficients. In the present study, a table lookup routine is incorporated to account for the effects of compressibility and static stall. Reverse flow is accounted for, and no small angle approximations are made in calculating the inflow angle and blade section angle of attack. This is because the lead-lag control concept is specifically designed to be effective at very high flight speeds where these angles would be expected to be large on the retreating side of the disk.

The 4/rev vibratory hub loads are calculated about a propulsive trim condition. Determining this trim condition requires the simultaneous solution of the blade flap-lag-torsion equations of motion and vehicle equilibrium equations. The flap-lag-torsion equations are solved using the Galerkin method. This enables the evaluation of the steady hub loads, which have an influence on the vehicle equilibrium. Solution of the vehicle equilibrium relations was carried out using the Newton-Raphson method to yield vehicle attitude and control settings. Since these, in turn, affect the blade response and steady hub loads, an iterative approach is adopted until both the response and the vehicle equilibrium equations are simultaneously satisfied. Vibratory hub loads are then calculated about this converged equilibrium condition.

To incorporate the effects of controlled lead-lag motions, the lag degree of freedom, ζ, can be decomposed into two parts: ζ_c (the controlled lag motions) and ζ_f (the free lag motions in response to the aerodynamic and inertial forces acting on the rotor blade). Thus,

$$\zeta_T = \zeta_f + \zeta_c \tag{4}$$

This is analogous to the case of torsion motions, where the total pitch angle comprises of an input control angle, θ, and a response, ϕ, to aerodynamic and inertial excitations. It is assumed that the lag spring and lag damper provide restoring moments proportional only to the free lag motions, ζ_f, and do not in any way resist the controlled lag motions, ζ_c. The modified lead-lag equation of motion can be expressed as

$$\ddot{\zeta}_T + \nu_\zeta^2 \zeta_T + 2\beta\dot{\beta} - 2I_x^*\beta\dot{\theta} + 2\xi\nu_\zeta\dot{\zeta}_T = \frac{M_\zeta^{aero}}{I_\beta\Omega^2} + \frac{K_\zeta}{I_\beta\Omega^2}\zeta_c + 2\xi\nu_\zeta\dot{\zeta}_c \tag{5}$$

This equation is identical in form to Eq. 2, with the exception of two additional terms on the right hand side related to the controlled lead-lag motions. The additional terms can alternatively be viewed as an equivalent lead-lag control moment acting on the blade. Thus, the blades can be subjected to controlled lead-lag motions, ζ_c, or a lag control moment,

$$\frac{M_c}{I_\beta\Omega^2} = \frac{K_\zeta}{I_\beta\Omega^2}\zeta_c + 2\xi\nu_\zeta\dot{\zeta}_c \tag{6}$$

the two being mathematically equivalent.

In the present study controlled lag motion inputs were considered, and were defined as follows:

$$\zeta_c = \bar{\zeta}_c \cos(n_c\psi - \phi_c) \tag{7}$$

where $\bar{\zeta}_c$ is the amplitude of the controlled lag motions, ϕ_c is the phase, and n_c denotes the harmonic of rotational speed.

Elastic Blade Model

An elastic blade rotor model was developed to predict rotor vibration. The coupled flap-lag-torsion equations of motion were developed based on the formulation found in Reference [15]. The rotor blades were modeled using finite element method to capture the elastic deformations in flap, lag, and torsion degrees of freedom. The aerodynamic model used is similar to the one used in the rigid blade model, except it accounts for elastic deformation and motion of the blades. The response of the blades is obtained using a finite element in time routine and is assumed to be the same for all blades. Using the response, the blade root loads and consequently the hub loads are calculated. Just as in the rigid blade model, the iterative Newton-Raphson method is used to solve for the helicopter control and attitude setting by simultaneously satisfying the vehicle trim equations and the response.

The lead-lag control was implemented using a lead-lag moment. Using a lag moment instead of lead-lag motion was deemed more practical due to ease of implementation. Only slight

modifications of the load vector were needed. The moment control was implemented by adding and subtracting the moment defined in Equation 8 to the lag degree of freedom of a chosen finite element.

$$M_c = \overline{M}_c \cos(n_c\psi - \phi_c) \tag{8}$$

The application of these moments to the finite element model is shown in Figure 3.

Results

In this section numerical results are presented on the influence of lead-lag control on helicopter vibrations for both the rigid blade and elastic blade models. For each model, vibration results are first presented for a rotor without lead-lag control. The vibration levels serve as a benchmark for comparisons with levels obtained when controlled lead-lag motions and moments are subsequently introduced.

Rigid Blade Results

Baseline Rotor

Figures 4 and 5 show the rotor vibratory loads as a function of the advance ratio, μ. An increase in vibration is discernible around $\mu = 0.3$, with levels starting to increase very rapidly past $\mu = 0.35$. Figures 6 and 7 show the vehicle attitude and control settings as a function of advance ratio. As with the vibration levels, some of the attitude and control settings show very large increases beyond $\mu = 0.35$. Figures 8 and 9 show the section angle of attack at any location on the rotor disk. The NACA 0012 airfoil used in this study stalls at around 15°. Figure 8 shows that at $\mu = 0.35$, there is a small region where the blade encounters stall on the retreating side of the disk. At $\mu = 0.4$, the stall region covers approximately half the rotor disk area, while negative angles of attack are observed on the advancing side. In addition to the drastic increase in vibration levels, this results in a phenomenal increase in the power requirements - from 2275 Hp, at $\mu = 0.35$, to 6595 Hp at $\mu = 0.4$. It should be noted that a 16,000 lb helicopter typically has an installed power in the range of approximately 2500 - 2800 Hp. Thus, while flight at $\mu = 0.35$ would be feasible, there would be insufficient power for flight at $\mu = 0.4$. An analysis of the

Table 1: Helicopter and rotor properties.

Weight	Radius, R	Chord, c
16,000 lbs	26.8 ft	1.75 ft
Solidity, σ	Number of blades, N	Hinge offset, e
0.08	4	1.25 ft
Nondimensional Rotating Frequencies		
1^{st} Flap	1^{st} Lag	1^{st} Torsion
1.07	0.7	7.0

high angles of attack on the retreating side at $\mu = 0.4$ revealed that the chief contributors were large values of collective pitch, longitudinal cyclic pitch, and the inflow angle (primarily due to large blade flapping).

1/rev Lead-Lag Control

Controlled lead-lag motions (Equation 7) are introduced at a frequency of 1/rev (n_c=1). Influence of phase, ϕ_c, and amplitude, $\bar{\zeta}_c$, of the controlled lag motions on the vibratory hub loads are first systematically examined to determine "optimum" controlled lag motions most effective for vibration reduction. At an advance ratio of $\mu = 0.4$, Figures 10-14 show the variations in individual components of 4/rev vibratory hub loads as a function of lead-lag control phase angle, ϕ_c, for different values of control motion amplitude, $\bar{\zeta}_c$. From these figures, it is clear that at $\phi_c = -100°$, all the vibrations are reduced substantially compared to the baseline (uncontrolled) levels. In general, as $\bar{\zeta}_c$ increases from 2° to 4°, larger vibration reduction can be achieved. However, it would also imply larger control effort and implementation difficulty. Further, it is seen that the vibratory vertical force and in-plane moments show relatively smaller reductions in vibration when $\bar{\zeta}_c$ increases from 3° to 4° (as compared to the reductions achieved when $\bar{\zeta}_c$ increased from 2° to 3°). Thus the lead-lag control settings selected in the present study were

$$\bar{\zeta}_c = 3° \quad \text{and} \quad \phi_c = -100°$$

For this 1/rev controlled lead-lag motion, the reduction in vibratory hub loads achieved at μ=0.4 (relative to the baseline uncontrolled rotor) are shown in Table 2. Reductions of up to 50% in hub forces, 75% in roll moment, and 30% in pitching moment were achieved. Table 3 compares the 4/rev vibratory hub loads at $\mu = 0.4$ in the presence of controlled lag motions to those of the baseline rotor at $\mu = 0.35$. Clearly, with the implementation of 1/rev controlled lead-lag motions, the vibratory loads at $\mu = 0.4$ are similar to values obtained at $\mu = 0.35$ for the baseline uncontrolled rotor.

Table 2: Percent reduction of vibratory hub loads using 1/rev controlled lag motions ($\mu = 0.4$).

Hub Load	F_x^{4P}	F_y^{4P}	F_z^{4P}	M_x^{4P}	M_y^{4P}
Reduction	50.2	44.5	44.7	74.0	27.6

Table 3: Vibratory hub loads (lbs and ft-lbs) for baseline rotor at $\mu = 0.35$ and a rotor with 1/rev controlled lag motions at $\mu = 0.4$.

Hub Load	F_x^{4P}	F_y^{4P}	F_z^{4P}	M_x^{4P}	M_y^{4P}
μ=0.35	589	584	1165	5731	2490
μ=0.4 (lag control)	596	617	1662	5475	8758

Table 4 shows the vehicle attitude and control settings at $\mu = 0.4$. As compared to the baseline rotor, it is seen that the 1/rev controlled lead-lag motions produce significant changes in the helicopter trim. Particularly significant are the reductions in main rotor collective pitch and longitudinal cyclic, tail rotor collective, and lateral shaft tilt angle. The blade section angle of attack at any location on the rotor disk is shown in Figure 15. The static stall region, so prominent in the baseline rotor (Fig. 9), is significantly reduced, with the smaller collective and longitudinal cyclic pitch settings most responsible for this reduction. It is this reduction in stall region due to change in trim that produces the significant vibration reductions seen in Table 2. The change in trim associated with 1/rev controlled lead-lag motions indicates that there should be changes in the steady rotor hub forces and moments. These are shown in Tables 5a and 5b, respectively.

Table 4: Vehicle attitude and control settings.

	α_s	ϕ_s	θ_o	θ_{1c}	θ_{1s}	θ_{tr}
Baseline	2.2	-12	18.6	3.8	-20.6	10.9
1/rev	1.9	-4.9	10.5	1.7	-12.5	4.3

Table 5a: Steady rotor hub forces (lbs).

	F_x^o	F_y^o	F_z^o
Baseline	-1318	-540	17609
1/rev	-1438	-201	17027

Table 5b: Steady rotor hub moments (ft-lbs).

	M_x^o	M_y^o	M_z^o
Baseline	-2282	-20214	-134077
1/rev	-513	-14999	-52507

To understand the impact of 1/rev controlled lead-lag motions on the steady (zeroeth harmonic) hub forces and moments, it should first be recognized that 1/rev components of inplane blade root shear forces (the radial shear, S_r, and drag shear, S_x) contribute to the inplane zeroeth harmonic steady hub forces, F_x^o and F_y^o. Similarly, the 1/rev component of blade root flapping moment, M_β, contributes to the inplane zeroeth harmonic steady hub moments, M_x^o and M_y^o. The controlled lead-lag motions directly affect the 1/rev components of S_r and M_β through the radial Coriolis force, and the 1/rev component of S_x through the lag acceleration force. Although, the controlled lead-lag motions initiate a change in the steady hub forces and moments via the inertial terms, the resulting change, itself, changes the aerodynamic environment and thus the aerodynamic components of the steady hub forces and moments are themselves significantly changed.

In Table 5b, a particularly significant reduction is observed in the steady hub torque, M_z^o. Again, this can be related to the reduced stall region on the retreating side of the disk (compare Figs. 15 and 9). The reduction in steady torque results in a drastic reduction in rotor power to a value of 2580 Hp (Compare to a value of 6595 Hp for the baseline rotor at $\mu = 0.4$). This value of rotor power falls well within installed levels typical of a 16,000 lb gross weight helicopter.

As compared to the baseline rotor, most flap-lag-torsion response harmonics decreased, a notable exception being the 1/rev lag response which increased by about 50% in amplitude and significantly changed phase. Reductions in the higher harmonic response and aerodynamic loads, caused by the new trim solution, together produced the decrease of the vibratory hub loads. The 1/rev controlled lag motions also produced a decrease in most blade root load harmonics. Notable exceptions here were the 1/rev components of blade root radial and drag shear which showed approximately 50% increases. This increase could have an impact on the blade fatigue life.

It is interesting to note that in contrast to the efforts of the late 1950's and early 1960's, reduction in vibratory hub loads was predicted using small-to-moderate lead-lag motion amplitudes. The vibration reduction was not achieved by equalizing the tangential velocity around the azimuth, but rather by changing the rotor trim such that the higher harmonic inertial and aerodynamic loads were reduced, particularly due to the reduction in stall region.

3/rev Lead-Lag Control

As seen in the previous section, the 1/rev controlled lead-lag motions were able to reduce vibrations by significantly altering the trim in high speed forward flight. Another way to reduce vibrations would be through the generation of higher harmonic unsteady loads that cancel the original loads responsible for producing the vibrations. This is similar, in principle, to vibration reduction using HHC, IBC, or Trailing Edge Flap actuation. One key difference is that in those cases unsteady aerodynamic loads are generated to cancel the vibrations. In the present case, controlled lead-lag motions would generate inertial loads to cancel the vibrations.

An examination of the effect of 3/rev controlled lead-lag motions on hub vibrations at $\mu = 0.4$, indicated that these controlled motions had an influence only on the inplane vibratory hub forces, F_x^{4P} and F_y^{4P}, and were unable to influence any of the other vibratory hub loads. Figures 16 and 17 show the variation in the inplane vibratory hub forces, as a function of controller phase, ϕ_c, for various amplitudes, $\bar{\zeta}_c$, of controlled 3/rev motions. From the figures it can be seen that both inplane vibrations are reduced at a phase angle of about -100°. When the lag control amplitude is increased beyond 0.5°, the vibrations appear to increase, suggesting that the system may be "overdriven" with the controlled motions actually producing vibrations rather than merely canceling them. Thus, the control settings selected for this case were,

$$\bar{\zeta}_c = \frac{1^\circ}{2} \quad \text{and} \quad \phi_c = -100^\circ$$

For these settings, the vibratory hub drag force, F_x^{4P}, was reduced by approximately 75% and the side force, F_y^{4P}, was reduced by 70%. Figures 18 and 19 show a vectorial decomposition of the vibratory hub loads into aerodynamic and inertial components, for the baseline rotor as well as the rotor with 3/rev controlled lag motions. While the aerodynamic loads are virtually unchanged, it is seen that introduction of 3/rev controlled lag motion decreases the amplitude of the inertial components, but more significantly, changes their phase, so that they counter the aerodynamic components and produce very small net vibratory loads. The effectiveness of 3/rev controlled lag motions in reducing hub inplane vibrations comes through its ability to directly influence the 3/rev components of blade root radial shear, S_r, and drag shear, S_x. The radial shear in influenced through the radial Coriolis force while the drag shear is influenced through the lag acceleration force.

The 3/rev controlled lag motions did not produce any significant change in rotor trim (or steady hub forces). The harmonics of blade response were not affected either, with the exception that the total third harmonic lag response decreased by 43%. The 3/rev controlled lag motions had no influence on the tangential velocity profile or blade angle of attack around the rotor disk. Thus, the static stall region was not reduced, and the power requirement for the main rotor remained at the unacceptably high level corresponding to the baseline case. Therefore, the 3/rev lead-lag control is not a good candidate for increase of maximum flight speed, but may be used to reduce the fairly high inplane vibratory loads at advance ratios prior to the onset of compressibility and stall. The lower motion amplitudes required would make implementation easier and the power requirements smaller than those for the 1/rev lag control concept.

Elastic Blade Model Results

In this section, results are presented for a study regarding the influence of lead-lag moment control on helicopter rotor vibration using an elastic blade model. The results for a baseline rotor, without lead-lag control, are presented and then compared to results obtained by introducing a lead-lag moment oscillating first at 1/rev and then 3/rev frequencies. Some of the vehicle and rotor properties are presented in Table 6.

Table 6 Helicopter and rotor properties.

Weight	Radius, R	Chord, c
6,200 lbs	16.2 ft	1.296 ft
Solidity, σ	Blade number, N	Lock Number, γ
0.1	4	6.34
Blade mass, m_o	Angular velocity, Ω	Airfoil
0.27 slugs/ft	40.123 rad/s	NACA 0012
Nondimensional Rotating Frequencies		
1st Flap	1st Lag	1st Torsion
1.11	0.61	3.29

Baseline Rotor

The vibration amplitudes for a baseline helicopter at increasing advance ratios is presented in Figures 20 and 21. The vibratory forces increase drastically above an advance ratio of 0.35. This is primarily due to a substantial growth of the retreating blade stall region (Compare Figures 22 and 23.) As this region grows, so does the steady torque, due to increase in drag, driving up the required power (See Figure 24). An increase in the advance ratio from 0.35 to 0.4 raises the rotor power from 523 Hp to 1215 Hp. These large increases in power and vibration impose a limit on the maximum advance ratio capability of the helicopter.

In the pervious section of this study, a rigid blade model was used to show that 1/rev lead-lag control can be utilized to increase the maximum advance ratio by reducing the vibration level and power required. Based on the insight gained from that analysis, it was necessary to double the mass per unit length, m_o, of the blades in order to increase the centripetal forces produced by the lead-lag moments. This increase in mass had a large affect on the ability of the lead-lag control to reduce vibration and reproduce the trends seen in the rigid blade study.

1/rev Lead-Lag Control

The rotor was actuated by a 1/rev lead-lag moment scheduled using Equation 8. Figure 26 presents the vibration levels for various amplitudes of the lead-lag moment, $\overline{M}_c$, versus the controller phase angle, ϕ_c, at an advance ratio of 0.4. These figures show that the maximum vibration reduction occurs near a phase angle of 0 degrees for a moment amplitude of 10,000 ft-lbs. The reductions in vibration are shown in Table 7.

Table 7 1/rev moment vibration reduction.

	F_x	F_y	F_z	M_x	M_y	M_z
% reduction	28.4	18.7	90.5	49.0	50.4	50.7

Examining the angles of attack for this case shows that the stall region is reduced (Compare Figures 23 and 25.) The maximum angle of attack decreases from almost 25 degrees to 19. The 1/rev lead-lag moment control creates small changes in the tip velocities, which do not significantly affect compressibility effects, but do have a substantial impact on the 1/rev blade root loads. The lag moment directly affects the inertial components of the 1/rev S_r and S_x blade root forces. These forces, when transformed into the fixed reference plane, produce the steady, in-plane hub forces which change the trim of the helicopter. This affects the aerodynamic loads, which further change the trim. The hub loads resulting from this change in trim are presented in Table 8. While the in-plane hub forces are dominated by the inertial loads, the moments are primarily affected by the aerodynamic loads. In particular, the change in steady torque can be attributed to a decrease in drag caused by a reduction in the retreating blade stall region. This can be directly linked to the changes in θ_o, θ_{1s}, and θ_{1c} shown in Table 9. With the exception of the forward shaft tilt, α_s, all the control settings and attitude angles are reduced in magnitude.

The change in steady torque causes a decrease in the rotor power. The baseline rotor required 1215 Hp to operate at an advance ratio of 0.4. The change in trim, caused by the 1/rev lead-lag moment, reduced the rotor power to 1000 Hp. The lead-lag actuation required another 7.4 Hp.

Therefore, even with the addition of the actuator, the total power to operate the 1/rev lead-lag rotor was lower than the total power of the unactuated rotor.

Table 8 Steady hub forces (lbs) and moments (ft-lbs).

	baseline			leadlag		
	total	inertial	aero	total	inertial	aero
F_x	-161	16.6	-177	-134	56.1	-190
F_y	-354	43.9	-398	-334	25.6	-360
F_z	6624	4.84	6619	6628	-1.15	6629
M_x	1508	793	715	1160	-262	1421
M_y	-4596	-556	-4041	-5051	-537	-4513
M_z	-16658	-17.1	-16641	-13681	-55.7	-13625

Table 9 Control settings (deg).

	θ_o	θ_{1c}	θ_{1s}	θ_{tr}	α_s	ϕ_s
Baseline	16.35	4.12	-14.77	10.06	4.43	-4.36
1/rev	14.53	3.47	-12.45	8.25	4.67	-3.21

3/rev Lead-Lag Control

The effects of the 3/rev lead-lag control were examined at an advance ratio of 0.3. Figure 27 shows the effect of 3/rev lead-lag control on the vibratory load at varying phase angles, ϕ_c. From these figures, it can be seen that a 3/rev moment of a magnitude of 300 ft-lbs, at a phase angle of −120 degrees produces significant vibration reduction in all the hub loads (See Table 10). Examining Figures 27(a-c) shows that the vibratory loads begin to increase for moments larger than 300 ft-lbs. This suggests that the system is being overdriven by the actuator.

Table 10 3/rev moment vibration reduction.

	F_x	F_y	F_z	M_x	M_y	M_z
% reduction	42.1	59.2	62.4	80.5	76.4	62.9

The effects of the 3/rev lead-lag moment on the angles of attack and air velocity are negligible. Likewise, the steady hub loads and trim are almost completely unaffected. Unlike the rigid blade model, which shows that the lead-lag control only affects the in-plane, 3/rev blade root forces, the elastic blade model predicts that the 3/rev moment affects other harmonics of all the blade root loads. See Table 11.

The components of the 4/rev hub loads have to be examined to determine the mechanism behind the vibration reduction. Figure 28 presents the vibratory hub loads using vector decomposition into inertial and aerodynamic components. The F_x^{4P} and F_y^{4P} hub forces (Figures 28 (a-b)) show that the 3/rev lead-lag moment does not affect the aerodynamic component of the in-plane hub forces, but it significantly influences their inertial components. The magnitude of the inertial components are decreased and change their phasing to be more out of phase with respect to the aerodynamic components. Both these effects reduce the in-plane hub forces.

Table 11 Non-dimensional blade root loads harmonics.

	0th	1st	2nd	3rd	4th	5th
S_r^{bl}	9.97e-1	5.28e-3	7.09e-4	4.01e-4	1.03e-4	3.73e-5
S_r^{ll}	9.97e-1	5.28e-3	7.14e-4	1.88e-4	9.10e-5	3.79e-5
S_x^{bl}	8.98e-3	4.08e-3	2.23e-4	2.20e-4	7.23e-5	1.03e-5
S_x^{ll}	8.98e-3	4.08e-3	2.29e-4	2.54e-4	2.43e-5	1.18e-5
S_z^{bl}	2.79e-2	7.74e-3	6.02e-3	6.49e-4	5.55e-5	6.75e-6
S_z^{ll}	2.79e-2	7.74e-3	6.04e-3	1.97e-4	2.09e-5	9.19e-6
M_ϕ^{bl}	7.04e-5	6.70e-5	1.83e-5	1.08e-5	2.37e-6	8.68e-7
M_ϕ^{ll}	7.04e-5	6.70e-5	1.84e-5	1.17e-5	2.06e-6	8.79e-7
M_β^{bl}	3.70e-3	1.08e-3	8.04e-4	8.56e-5	6.33e-6	8.66e-7
M_β^{ll}	3.70e-3	1.08e-3	8.09e-4	2.79e-5	5.20e-6	1.31e-6
M_ζ^{bl}	1.49e-3	9.76e-4	5.49e-5	2.35e-5	1.40e-5	1.60e-6
M_ζ^{ll}	1.49e-3	9.76e-4	5.58e-5	5.24e-5	5.18e-6	1.87e-6

The thrust vibratory load, F_z^{4P}, is reduced despite a 12 percent increase in the inertial component and a slight increase in the aerodynamic component, because the two components are more out of phase with respect to each other and cancel each other out. The rolling moment, M_x^{4P}, and the pitching moment, My_x^{4P}, both have a slight increase in the aerodynamic components and a small decrease in the inertial components. The change in phasing of these components produces a significant decrease in total vibratory loads, because the components act almost 180 degrees out of phase. The 3/rev lead-lag moment control creates a large reduction in the vibratory torque, M_z^{4P}, through a decrease in both the inertial and aerodynamic components and improved phasing between them.

The power required to operate the rotor did not decrease, as it did in the 1/rev lead-lag control case. The 3/rev lead-lag moment did not change the trim of the helicopter, or the tip velocities, leaving the power required to spin the rotor at 402 Hp. The lead-lag actuator required less than 0.1 Hp to produce the 3/rev moment required.

Conclusions

The effectiveness of controlled 1/*rev* and 3/*rev* lead-lag motions for vibration reduction and possible flight envelope expansion was investigated using two different analytical models. First, a rigid blade model was used to obtain a basic understanding the physics governing the lead-lag control problem and to explore the possibility of using lead-lag motions/moments for vibration reduction. The second, an elastic blade rotor model,

was used to confirm the results of the rigid blade study and to obtain a more accurate representation of the vibratory behavior of the rotor with lead-lag control. Several conclusions can be reached from this study.

1. 1/rev lead-lag control showed the ability to reduce vibratory loads and power required at an advance ratio of 0.4 to near $\mu = 0.35$ levels. Therefore, 1/rev lead-lag control may be a possible method to expand the flight envelope of a helicopter.

2. The 1/rev lead-lag control reduces rotor vibration by changing the trim of the helicopter which drastically reduces the retreating stall region of the helicopter. This change affects the response of the blades and the higher harmonic aerodynamic and inertial loads. This effect was predicted by both the rigid and elastic blade models.

3. The large reduction of the retreating stall region by the 1/rev lead-lag control also produced a significant reduction of the rotor power which offset the increase in power due to the lead-lag control implementation.

4. The elastic blade model showed the significance of the mass on the effectiveness of 1/rev lead-lag control. The blades must have sufficient amount of mass in order to effect the trim of the helicopter.

5. The rigid blade model predicted that both the 1/rev and 3/rev controlled lead-lag motions affected the radial Coriolis force and the lag acceleration force.

6. The rigid blade model showed that 3/rev lead-lag control affects only the in-plane vibratory forces, while the elastic blade predicted reductions in most hub loads. This discrepancy aside, both models showed that 3/rev lead-lag control does not affect the trim, but cancels out the vibratory loads using changes in the 3/rev inertial loads in a manner similar to HHC and IBC where aerodynamic forces are used.

The basic idea of lead-lag control was shown to reduce the vibratory hub loads at high advance ratios. The largest problem that needs to be overcome in implementation of this concept is actuation. Current actuator technology may not be able to provide the moment amplitudes required to actuate the blades in an actuator that is practical to install on a rotor blade.

References

[1] King, S. P., The Westland Rotor Head Vibration Absorber Design Principles and Operational Experience, Vertica, Vol. 11 (3), 1987.

[2] Amer, K. B., Neff, J. R., Vertical-Plane Pendulum Absorbers for Minimizing Helicopter Vibratory Loads, Journal of the American Helicopter Society, October 1974.

[3] Paul, W. F., Development and Evaluation of the Main Rotor Bifilar Absorber, Proceedings of the 25th Annual Forum of the American Helicopter Society, Washington, DC, May 1975.

[4] Drees, J. M., Wernicke, R. K., An Experimental Investigation of a Second Harmonic Feathering Device on the UH-1A Helicopter, U.S. Army Transportation Rese-arch Command, TR-62-109, Fort Eustis, Virginia, June 1963.

[5] Robinson, L. H., Lawson, H., Friedmann, P. P., Aeroelastic Simulation of Higher Harmonic Control, NASA-CR-4623, 1994.

[6] Powers, R. W., Preliminary Design Study of A Higher Harmonic Blade Feathering Con-trol System, NASA-CR-159327, June 1980.

[7] Ham, N. D., Helicopter Individual-Blade-Control: Promising Technology for the Fut-ure Helicopter, Proceedings of the American Helicopter Society Aeromechanics Confe-rence, Bridgeport, Connecticut, October 1995.

[8] Celi, R., Friedmann, P. Aeroelastic Modeling of Swept Tip Rotor Blades Using Finite Elements, Proceedings of the 43rd Annual Forum of the American Helicopter Society, St. Louis, Missouri, May 1987.

[9] Stroub, R., Rabbott, J., Jr., Niebanck, C. Rotor Blade Tip Shape Effects on Performance and Control Loads from Full-Scale Wind Tunnel Testing, Journal of the American Helicopter Society, October 1979.

[10] Desopper, A., Lafon, P., Céroni, P., Philippe, J. J. Ten Years of Rotor Flow Studies at ONERA, Journal of the American Helicopter Society, January 1989.

[11] Rangacharyulu, M. A., Moore, M. Flight Vibration Testing of the V-22 Tiltrotor Aircraft, Proceedings of the 47th Annual Forum of the American Helicopter Society, Phoenix, Arizona, May 6-8, 1991.

[12] Jenney, D. A Summary of the Lagging Rotor Program, United Aircraft internal document, April 2, 1959.

[13] Jenney, D. Preliminary Analysis of a Proposed Method for Increasing the Forward Speed of Helicopters – Project 15122, United Aircraft internal document, November 27, 1956.

[14] Derschmidt, H. High-Speed Rotor with Blade-Lag Motion Control, Institute of the Aerospace Sciences 31st Annual Meeting, New York, New York, January 21-23, 1963.

[15] Big G., Chopra I., et al University of Maryland Advanced Rotorcraft Code (UMARC) Theory Manual, UM-AERO Report 92-02 Aug 1992

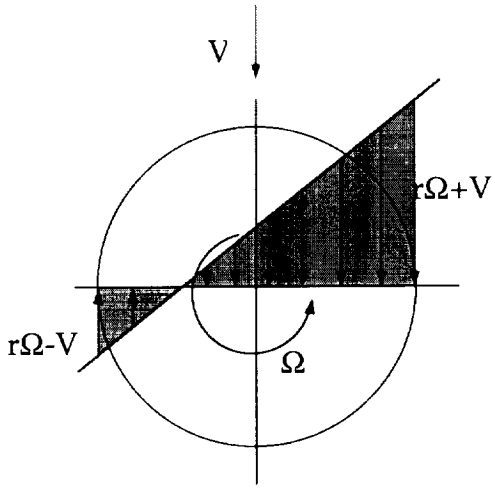

Figure 1: Tangential velocity profile in forward flight for conventional rotor.

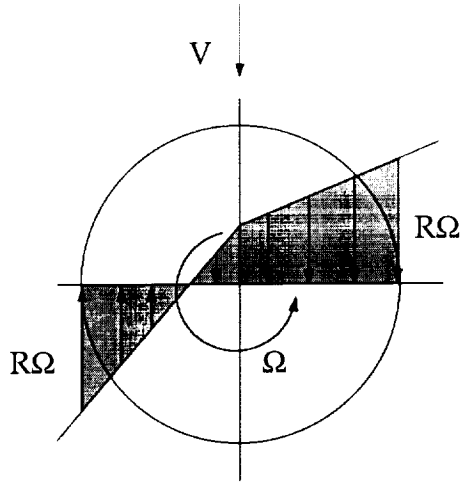

Figure 2: Tangential 1/*rev* velocity profile in forward flight with lead-lag control.

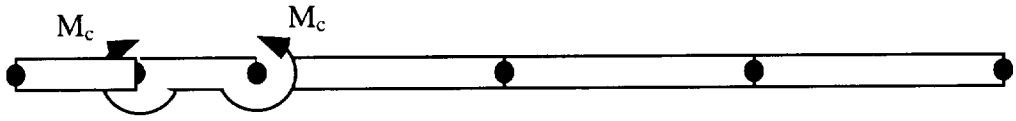

Figure 3. Application of lead-lag moment to finite element model.

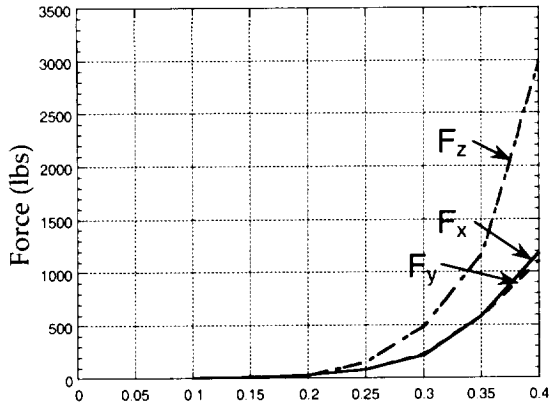

Fig. 4: Vibratory forces of baseline rotor versus advance ratio.

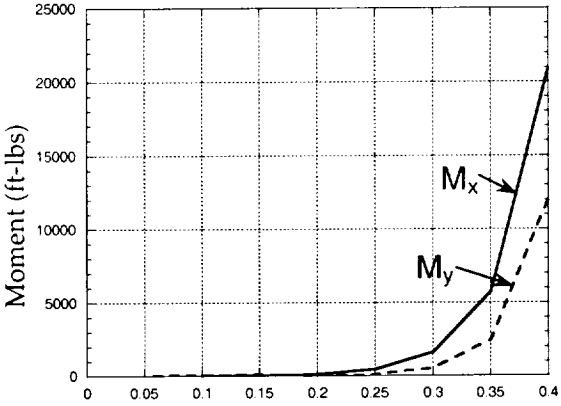

Fig. 5: Vibratory moments of baseline rotor versus advance ratio.

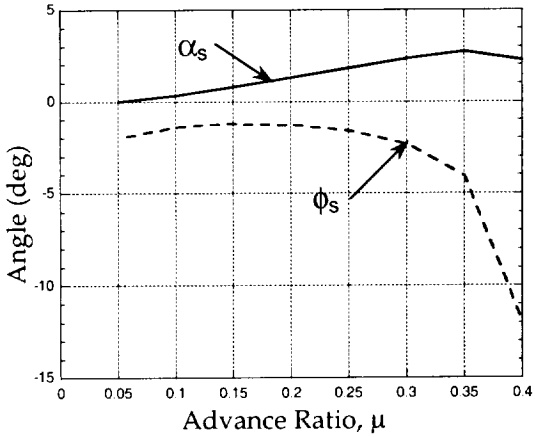

Fig. 6: Helicopter attitude angles versus advance ratio.

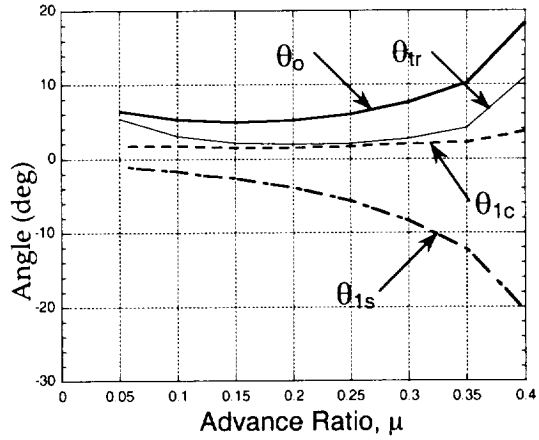

Fig. 7: Baseline rotor control settings versus advance ratio.

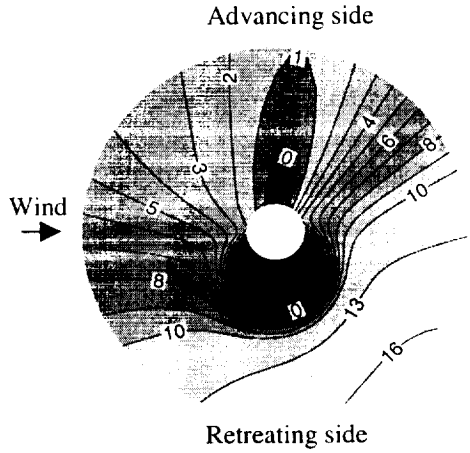

Fig. 8: Angle of attack at any location on rotor disk (baseline rotor, μ=0.35).

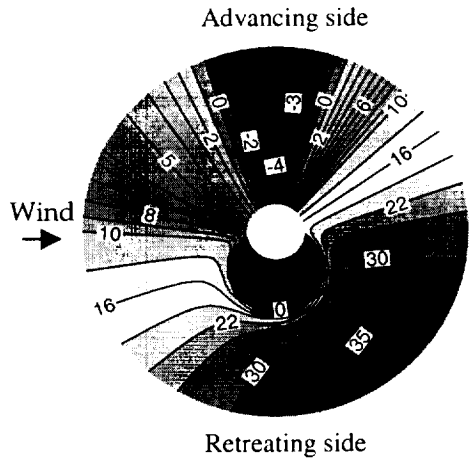

Fig. 9: Angle of attack at any location on rotor disk (baseline rotor, μ=0.4).

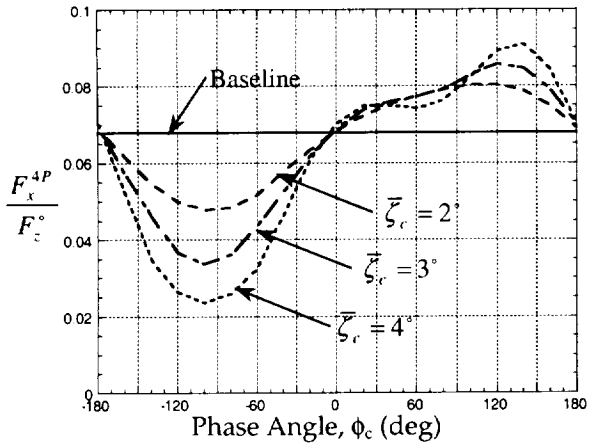

Fig. 10 Vibratory hub drag force versus 1/*rev* lag control phase angle, ϕ_c (μ = 0.4).

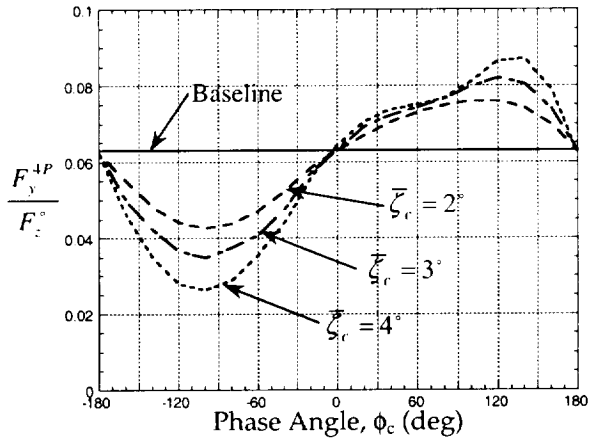

Fig. 11: Vibratory hub side force versus 1/*rev* lag control phase angle, ϕ_c (μ = 0.4).

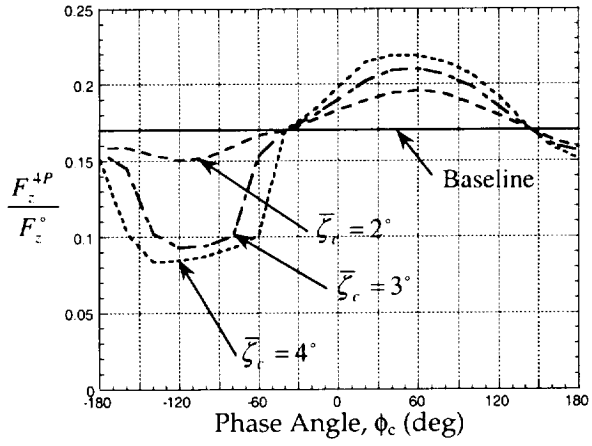

Fig. 12: Vibratory hub vertical force versus 1/*rev* lag control phase angle, ϕ_c (μ = 0.4).

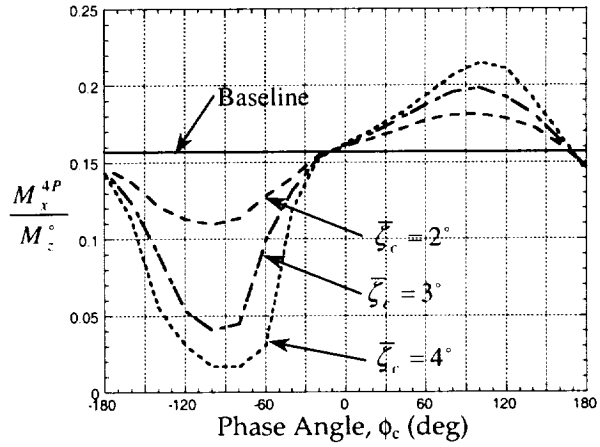

Fig. 13: Vibratory hub rolling moment versus 1/*rev* lag control phase angle, ϕ_c (μ = 0.4).

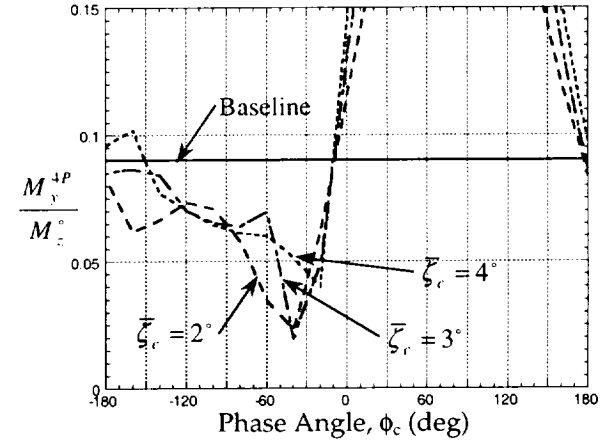

Fig. 14: Vibratory hub pitching moment versus 1/*rev* lag control phase angle, ϕ_c (μ = 0.4).

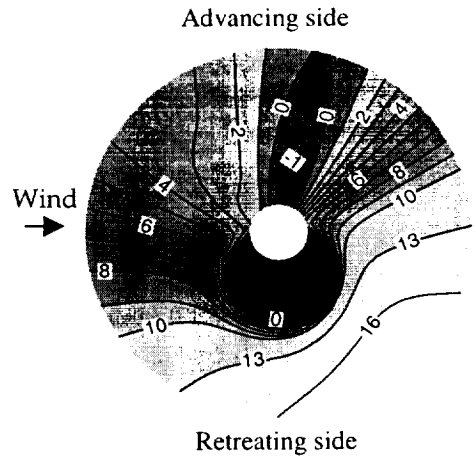

Fig. 15: Angle of attack at any location on rotor disk (1/*rev* lag control, μ=0.4).

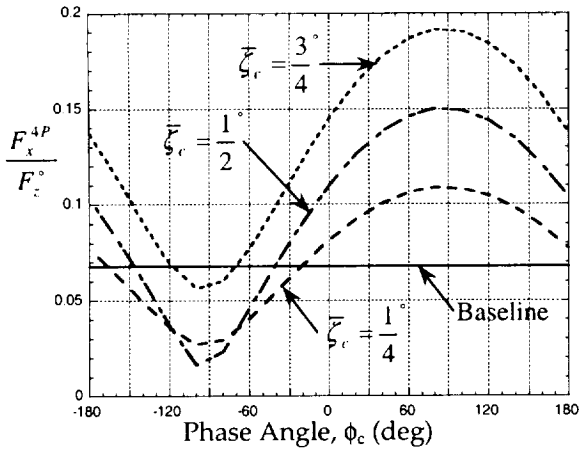

Fig. 16: Vibratory hub drag force versus 3/*rev* lag control phase angle, ϕ_c (μ = 0.4).

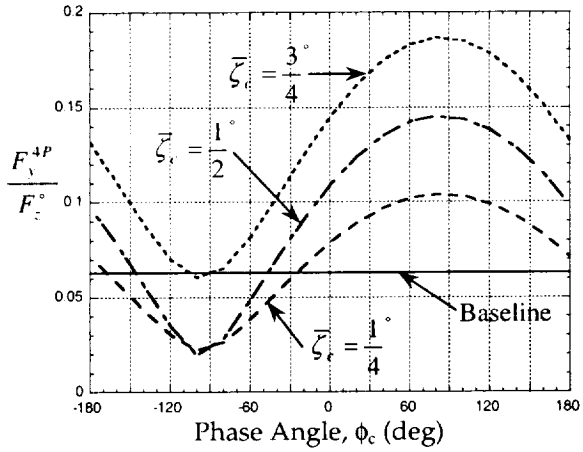

Fig. 17: Vibratory hub side force versus 3/*rev* lag control phase angle, ϕ_c (μ = 0.4).

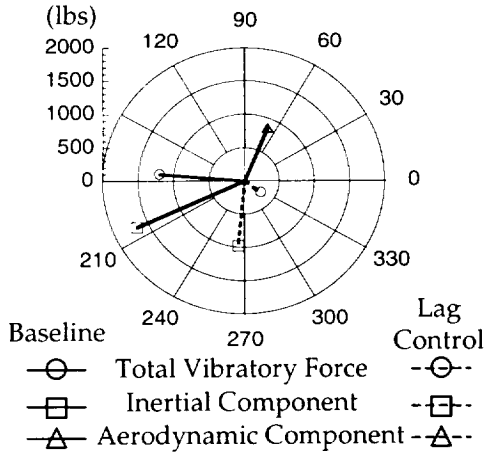

Fig. 18: Vectorial decomposition of vibratory hub drag force, F_x^{4P}, for a baseline and 3/*rev* lag control rotor (μ = 0.4).

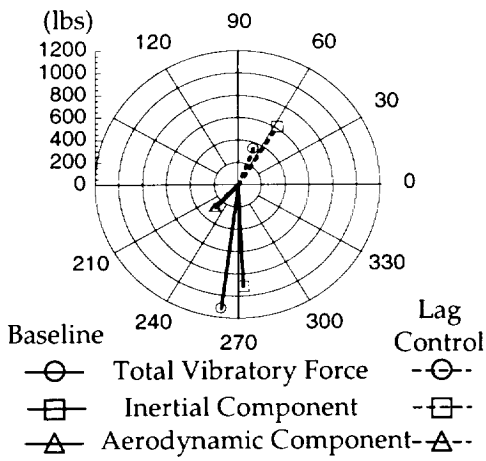

Fig. 19: Vectorial decomposition of vibratory hub side force, F_y^{4P}, for a baseline and 3/*rev* lag control rotor (μ= 0.4).

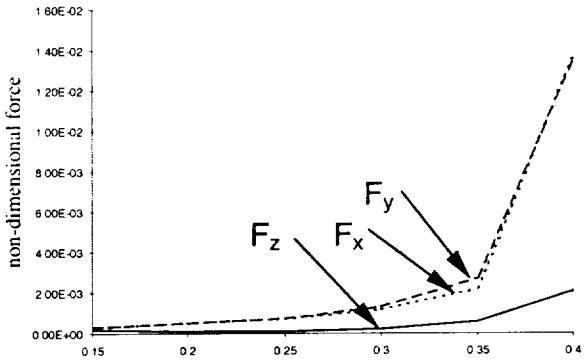

Fig. 20 Baseline vibratory hub forces vs. advance ratio.

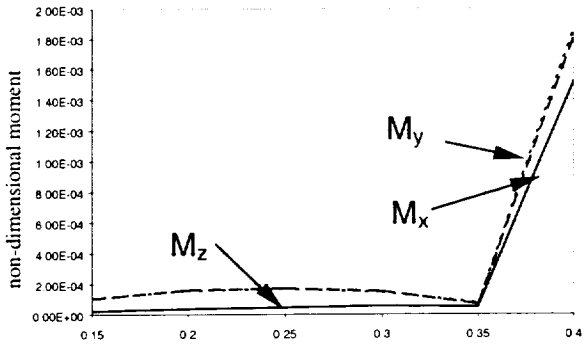

Fig. 21 Baseline vibratory hub moments vs. advance ratio.

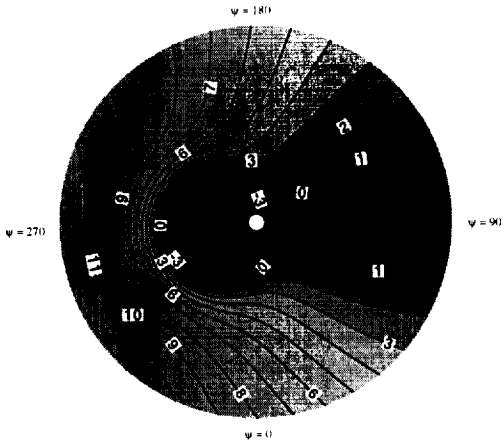

Figure 22 Angles of attack vs. rotor disk location at $\mu = 0.35$.

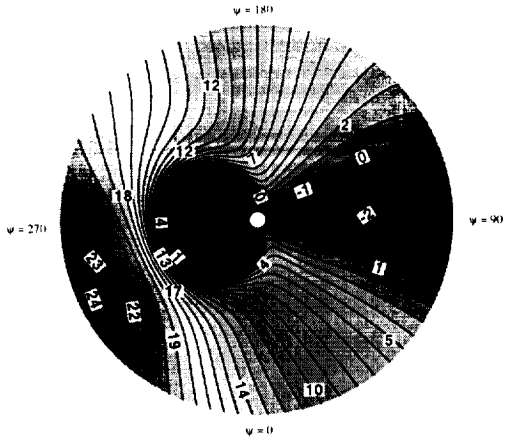

Figure 23 Angles of attack vs. rotor disk location at $\mu = 0.4$.

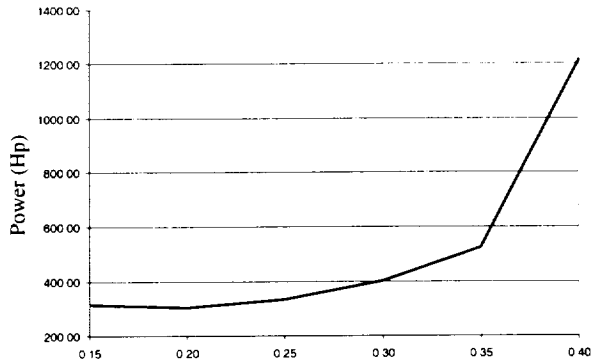

Figure 24 Rotor power vs. advance ratio.

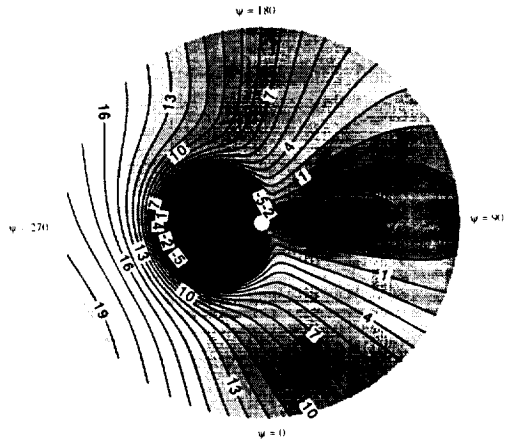

Figure 25 Angles of attack vs. rotor disk location at $\mu = 0.4$ for M_c = 10000 ft-lbs and $\phi_c = 0$ deg.

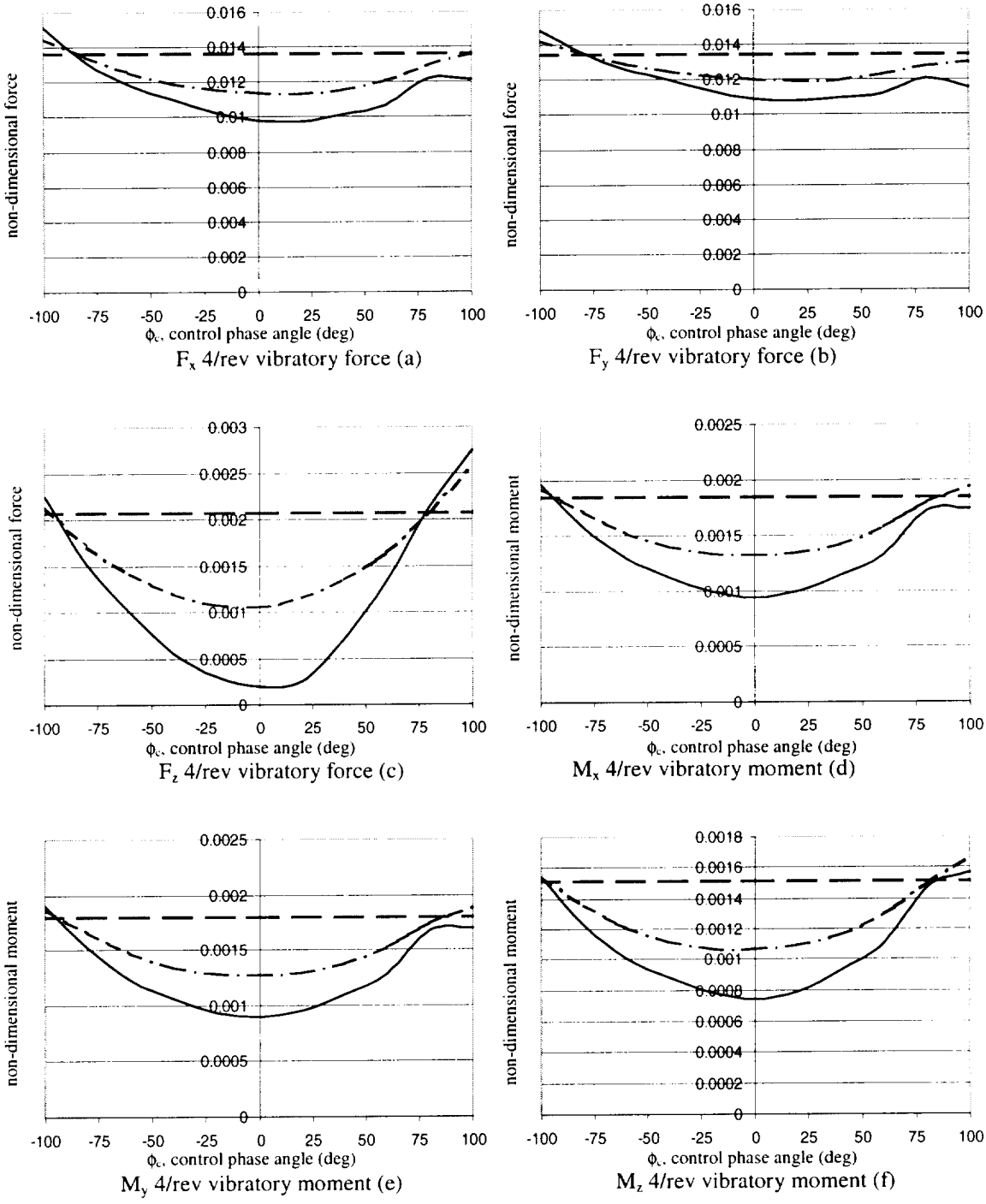

Figure 26 (a-f) Hub 4/rev vibratory loads due to 1/rev control moment at μ=0.4.

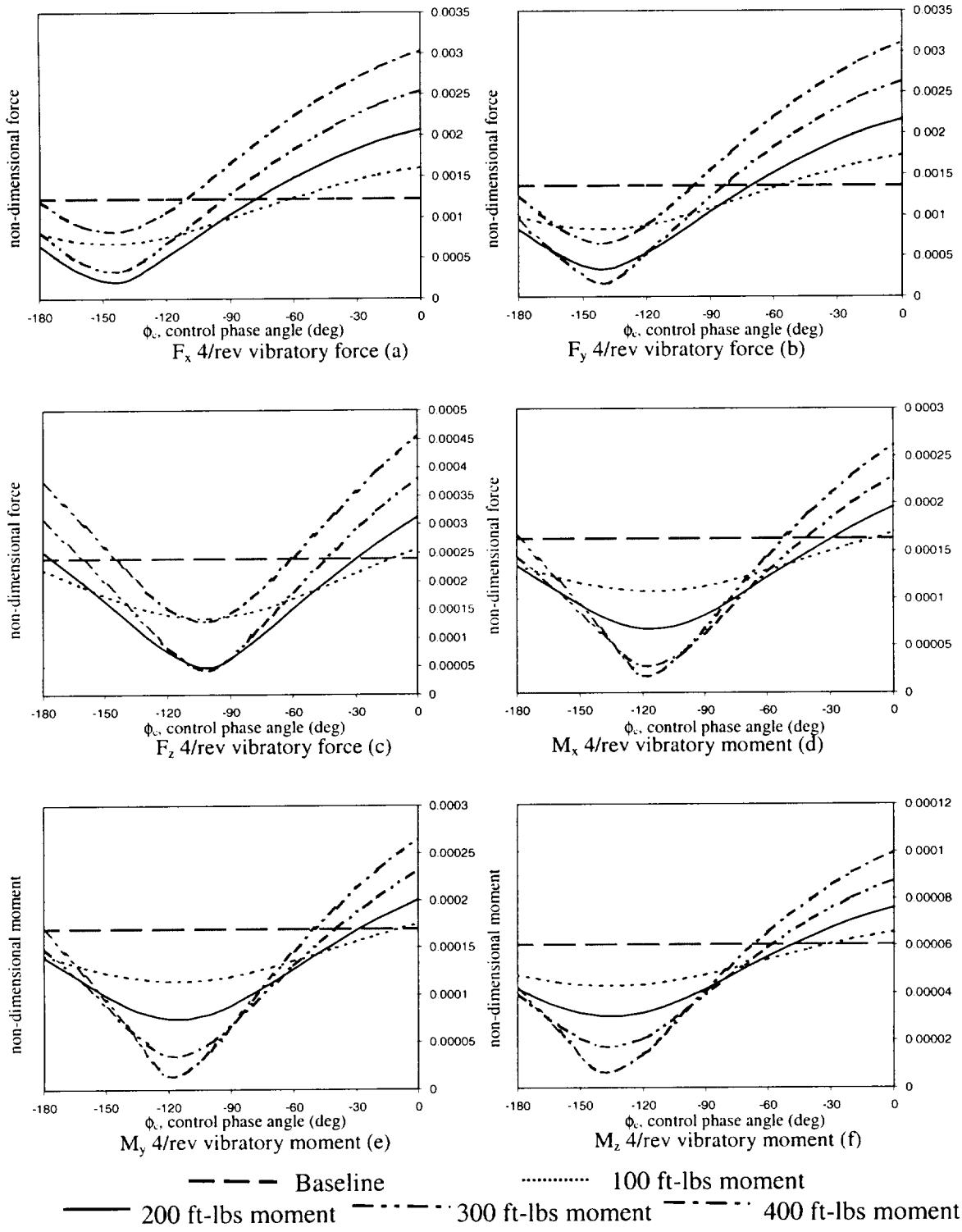

Figure 27 (a-f) Hub 4/rev vibratory loads due to 3/rev control moment μ=0.3.

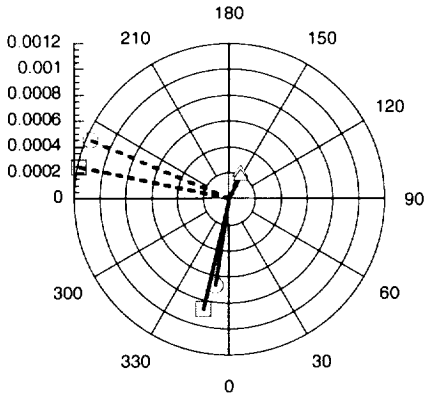

(a) F_x

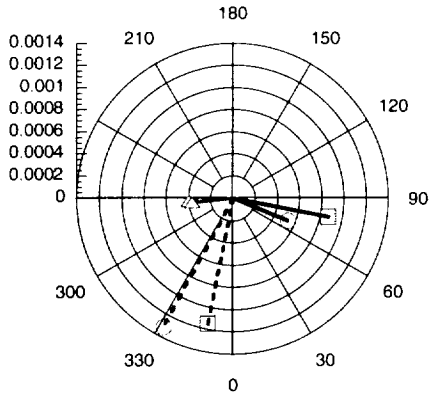

(b) F_y

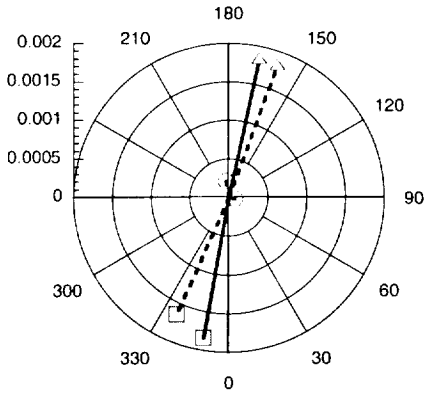

(c) F_z

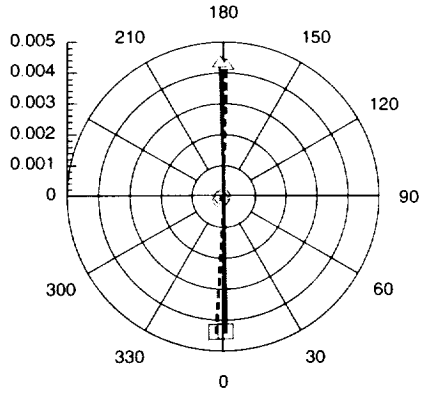

(d) M_x

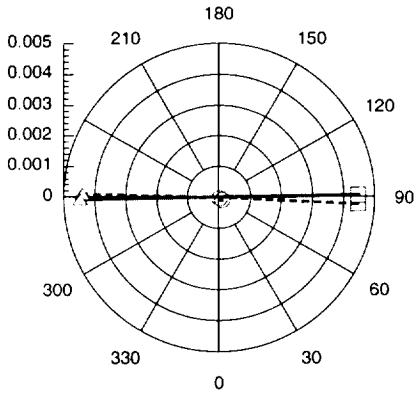

(e) M_y

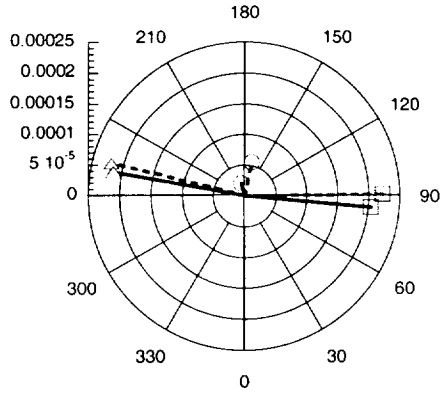

(f) M_z

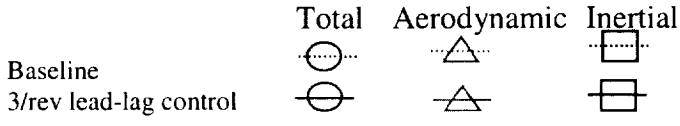

Figure 28(a-f) 4/rev hub load decomposition.